Research Square

Preprints are preliminary reports that have not undergone peer review.
They should not be considered conclusive, used to inform clinical practice,
or referenced by the media as validated information.

Enhancing the photostability of rhodamine 6G under laser irradiation with phenolic additives: Effects of electron-donating/withdrawing characteristics of para substituents

Runxin Wang
East China University of Science and Technology
Liang Sun
Research Institute of Physical and Chemical Engineering of Nuclear Industry
Yudong Liu
Research Institute of Physical and Chemical Engineering of Nuclear Industry
Jinlong Zhang
East China University of Science and Technology
Baozhu Tian
baozhutian@ecust.edu.cn

East China University of Science and Technology

Research Article

Keywords: Phenols, Photostability, Electron-donating/withdrawing substituent, Singlet oxygen quenching, Electronic transfer

Posted Date: November 26th, 2026

DOI: https://doi.org/10.21203/rs.3.rs-11692057/v1

License: This work is licensed under a Creative Commons Attribution 4.0 International License.
Read Full License

Additional Declarations: No competing interests reported.

Enhancing the photostability of rhodamine 6G under laser irradiation with phenolic additives: Effects of electron-donating/withdrawing characteristics of para substituents

RunxinWang [1], Liang Sun [2], Yudong Liu [2], Jinlong Zhang [2], Baozhu Tian [1]

[a] *State key laboratory of green chemical engineering and industrial catalysis, Shanghai Engineering Research Centre for Multi-media Environmental Catalysis and Resource Utilization, Key Laboratory of Specially Functional Polymeric Materials and Related Technology (Ministry of Education), Key Laboratory for Advanced Materials and Joint International Research Laboratory of Precision Chemistry and Molecular Engineering, School of Chemistry and Molecular Engineering, East China University of Science and Technology, 130 Meilong Road, Shanghai 200237, PR China*

[b] *Research Institute of Physical and Chemical Engineering of Nuclear Industry, 168 JinTang Road, Tianjin, 300180, PR China*

Corresponding author: *baozhutian@ecust.edu.cn.*

Abstract

The addition of phenolic antioxidants is an effective strategy to improve the photostability of fluorescent dyes. Nevertheless, the regularities and mechanisms by which substituent electronic properties control photoprotective efficacy remain unclear. Herein, we investigated how electron-donating/withdrawing substituents affect photostability enhancement, using five para-substituted phenols, i.e., p-hydroxybenzoic acid (PHBA), p-cyanophenol (PCP), phenol (PhOH), p-ethylphenol (PEP), p-aminophenol (PAP) as targets and Rh6G photobleaching under 532 nm laser irradiation as the probe reaction. Their photobleaching-suppressing efficacy follows: PAP > PEP > PhOH > PCP > PHBA, i.e., the protective efficacy rises as the Hammett constant (σ_p) decreases. EPR and ABDA measurements identify singlet oxygen ($^1O_2$) as the dominant reactive oxygen species. DFT calculations reveal $^1O_2$ is chemically quenched mainly via 1,3-addition, with barriers falling from 38.8 (PHBA), 37.5 (PCP), 36.2 (PhOH), 35.1 (PEP) to 31.5 kcal mol^{-1} (PAP). Cyclic voltammetry and HOMO analyses show that phenols with stronger reducing power react faster with $^1O_2$ and better suppress dye photobleaching. Fluorescence correlation spectroscopy further confirms Rh6G triplet population declines as the electron-donating character of para-substituents increases. Specifically, phenols protect Rh6G via a sacrificial antioxidant pathway: they are preferentially oxidized to scavenge $^1O_2$. Stronger electron-donating para-substituents reduce the activation barrier between phenols and $^1O_2$, accelerating the reaction and improving photoprotection. This work clarifies how phenolic substituent electronic properties tune photostabilizing performance and guides the rational design of phenolic photostabilizers.

Keywords: Phenols; Photostability; Electron-donating/withdrawing substituent; Singlet oxygen quenching; Electronic transfer

1 Introduction

Organic fluorescent dyes are widely utilized in fluorescent probes [1–3], optoelectronic devices [4, 5], and laser media [6–8], owing to their broad fluorescence emission range, high quantum yield, and tunable luminescent wavelengths [3, 9–11]. Nonetheless, these fluorophores tend to undergo severe photobleaching upon prolonged irradiation [12], which substantially curtails their service lifespan and practical usability. To address this undesirable degradation behavior, a series of tailored strategies have been developed to suppress dye photobleaching, including molecular structural modification [13–17], encapsulation within inert protective matrices [18, 19], and incorporation of external stabilizing agents [20]. Among these available techniques, the introduction of external stabilizers is highly favored, due to its straightforward operation and negligible disturbance on the intrinsic spectral characteristics of fluorescent dyes.

To date, a variety of functional stabilizers have been exploited to enhance the photostability of organic fluorescent dyes, including antioxidants (propyl gallate, ascorbic acid) [21–23], triplet quenchers (cyclooctatetraene) [24], photolysis inhibitors (benzotriazole) [25], and metal ion chelators for suppressing adverse effects of Fe and Ni [26]. Among these candidates, phenolic antioxidants have attracted substantial research attention owing to their efficient radical-scavenging capability, low biological toxicity, and eco-friendly characteristics, making them a research hotspot in dye photostability modification. For example, Gamage et al. demonstrated that the introduction of α-tocopherol effectively alleviated the photobleaching of photochemically unstable indocyanine green, nearly tripling the service life of the dye [27]. Similarly, Giloh et al. found that n-propyl gallate could reduce the fluorescence fading rate of tetramethylrhodamine by an order of magnitude [21]. Moreover, Aitken et al. presented the improved stability of dyes in the protocatechuic acid/protocatechuate-3,4-dioxygenase O_2-scavenging system [23]. In our previous study, we systematically compared the photoprotective effects of multiple phenolic compounds (catechinic acid, n-propyl gallate, caffeic acid, and chlorogenic acid) on Rh6G. The results confirmed that the photostabilization efficiency of these phenols is inherently governed by their intrinsic reducing capacity [28].

Although the aforementioned studies have verified the favorable effects of phenolic compounds on enhancing the photostability of fluorescent dyes, the underlying structure–activity relationships and intrinsic mechanisms by which structural characteristics, particularly aromatic substituent properties,

modulate photoprotective efficiency remain to be further clarified. For phenolic molecules, benzene ring substituents can significantly alter the molecular electronic microenvironment. Specifically, electron-donating groups (EDGs) and electron-withdrawing groups (EWGs) exert a crucial influence on the electronic configuration and electrostatic potential (ESP) of phenolic molecules [29, 30]. Accordingly, it is essential to systematically explore how the electronic properties of phenolic substituents dominate the photostabilization performance of fluorescent dyes.

In this work, we systematically investigated how the electronic properties of para substituents in phenolic derivatives govern the photostability of fluorescent dyes, using the photobleaching of rhodamine 6G (Rh6G) as a probe reaction. Five phenolic compounds, namely p-hydroxybenzoic acid (PHBA), p-cyanophenol (PCP), phenol (PhOH), p-ethylphenol (PEP) and p-aminophenol (PAP), were chosen as model systems (Fig. 1), and their electron-donating and electron-withdrawing characteristics were quantified via Hammett substituent constants (σ_P). Electron paramagnetic resonance (EPR) spectroscopy and reactive oxygen species (ROS) trapping assays were performed to identify the dominant ROS species responsible for Rh6G photobleaching. We calculated the Gibbs free energy change (ΔG) to assess the thermodynamic spontaneity of ROS-triggered reactions between phenolic molecules and ROS, whereas the Gibbs free energy of activation ($\Delta G‡$) was adopted to evaluate the kinetic reaction rate of such processes. Cyclic voltammetry (CV) measurements combined with HOMO energy level calculations were used to compare the reducing capacity of these phenolic derivatives. Furthermore, fluorescence correlation spectroscopy (FCS) was applied to characterize how various phenolic compounds alter the fraction of Rh6G molecules residing in the triplet excited state (T_1). Integrating all the above experimental characterizations and theoretical computational results, we elucidated the underlying structure–activity relationship and intrinsic mechanisms by which the electronic features of para substituents tune the photostability of Rh6G.

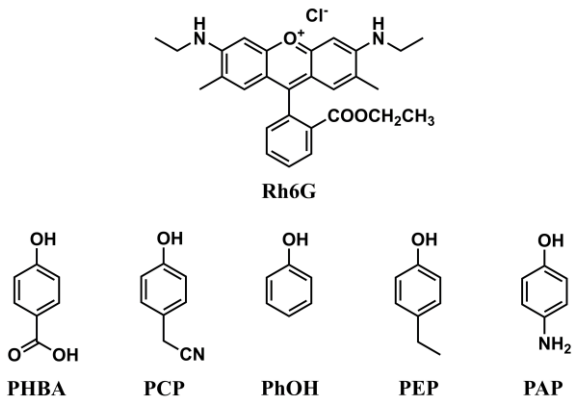

Fig. 1. Chemical structures of the Rh6G and the phenols

2 Experimental sections

2.1 Materials

Rhodamine 6G chloride (Rh6G) and 9,10-anthracenediyl-bis(methylene)dimalonic acid (ABDA) were purchased from TargetMol Chemicals Inc. *p*-hydroxybenzoic acid (PHBA), *p*-cyanophenol (PCP), phenol (PhOH), *p*-ethylphenol (PEP), *p*-aminophenol (PAP), ethanol, methanol, 2,2,6,6-tetramethyl-piperidin (TEMP), and 5,5-dimethyl-1-pyrroline-N-oxide (DMPO) were supplied by Shanghai Titan Scientific Co., Ltd. Sodium hydroxide (NaOH), terephthalic acid (TA), sodium 2,3-bis(2-methoxy-4-nitro-5-sulfophenyl)-2H-tetrazolium-5-carboxanilide inner salt (XTT), 2,2'-diphenyl-1-picrylhydrazyl (DPPH), and tetrabutylammonium hexafluorophosphate ($TBAPF_6$) were obtained from Shanghai Aladdin Holdings Group Co., Ltd. All chemicals were of analytical grade and used as received without further purification.

2.2 Photostability measurements

The photostability measurements were performed on a home-built photostability test setup (Fig. S1), which consisted of a solid-state laser (wavelength: 532 nm; repetition frequency: 10 kHz; pulse width: 50 ± 10 ns), a dye circulation system (including a circulation pump, quartz-jacketed dye storage tank and circulation pipelines), a cooling system (water chiller and cooling circulation pipelines), and a dye cell equipped with quartz windows. The test solutions were prepared with methanol and water with a volume ratio of 1:4, and the concentrations of Rh6G and phenolic additives were 0.3 mM and 0.6 mM, respectively. The experimental procedure was as follows: the solid-state laser was turned on, and the laser beam direction was adjusted to irradiate vertically the middle position of the quartz window of the dye cell. The laser output power was set to 45 W. A total of 150 mL of the test solution was added into

the dye circulation system, followed by switching on the dye circulation pump and cooling water pump to maintain the solution temperature at a constant 25 ℃. Afterwards, the laser baffle was removed to initiate the photostability test. At regular time intervals, 1 mL of the solution was sampled, and the residual dye concentration was determined using a UV–visible spectrophotometer. The dye residual rate was calculated based on the variation in absorbance at the maximum absorption wavelength using Eq. 1:

$$Dye\ Residual\ Rate = \frac{A_t}{A_0} \times 100\% \quad \text{(Eq. 1)}$$

where A_0 and A_t represent the absorbance values before irradiation and after t h of irradiation, respectively.

2.3 Analysis of ROS with EPR

Reactive oxygen species (ROS) were detected using a Bruker EMX-8 X-band electron paramagnetic resonance (EPR) spectrometer. For the $^1O_2$ analysis, 50 μL of TEMP was added to 1 mL of aqueous solution containing 5 μM Rh6G and 100 μM phenols. The mixture was irradiated with 525 nm LED light for 1 min, transferred to a quartz capillary, and immediately inserted into the EPR cavity for testing. Hydroxyl radicals (•OH) and superoxide radicals ($•O_2^-$) were probed with DMPO as the spin-trapping agent. Specifically, •OH was measured in an aqueous system, whereas $•O_2^-$ assayed in methanol solution. Dark control experiments were implemented to identify the role of light in ROS generation.

2.4 Estimation of the generation rate of $^1O_2$ via ROS trapping experiments

To quantify the ROS generation rate in different phenolic additive systems under light irradiation, the ROS trapping experiments were carried out. Herein, the $^1O_2$ generation rate was estimated using ABDA as trapping agent and the detailed experimental procedures are described as follows: An Methanol–water mixture (20:80, v/v) containing 50 μM ABDA, 5 μM Rh6G and 100 μM phenols was irradiated with 525 nm LED light. At specific time intervals, Aliquots were collected and their absorbance at 378 nm was recorded using a UV-Vis spectrophotometer (Shimadzu UV-2600i). Since the decomposition rate of ABDA is proportional to $^1O_2$ yield, the $^1O_2$ yield can be estimated from the ABDA degradation rate, which was calculated according to Eq. 2.

$$ABDA\ scavenging\ rate(\%) = 1 - \frac{A_t}{A_0} \times 100\% \quad \text{(Eq. 2)}$$

Since TA reacts with •OH to produce the fluorescent product 2-hydroxyterephthalic acid (TAOH), which exhibits maximum fluorescence emission at 425 nm, TA was employed as a fluorescent probe to quantify the •OH generation rate. The experimental procedure is described below: A 100 mL alkaline

aqueous mixture consisting of 500 μM TA, 2 mM NaOH, 5 μM Rh6G and 100 μM phenolic additives was irradiated with 525 nm LED light. At specific time intervals, aliquots were withdrawn and their fluorescence intensities at 425 nm were measured on an Edinburgh FLS980 fluorescence spectrometer.

XTT reacts with $\bullet O_2^-$ to yield water-soluble orange formazan (λ_{max} = 470 nm), the production rate of $\bullet O_2^-$ was quantified by monitoring the absorbance variation at 470 nm. For each measurement, a 100 mL aqueous mixture containing 50 μM XTT, 5 μM Rh6G and 100 μM phenolic additives was irradiated with 525 nm LED light. At scheduled time intervals, aliquots were withdrawn for absorbance measurement at 470 nm.

2.5 Computational Methods

Density functional theory (DFT) calculations were carried out with Gaussian 09 to explore the electronic structures of phenols and their reaction behaviors toward ROS. Geometric optimizations and vibrational frequency calculations for phenols, reactant complexes (RC), transition states (TS), and products (P) were performed at the M06-2X/6-311G (d, p) level, while the single-point energy was refined at M062X/def2TZVP level [31–33]. Intrinsic reaction coordinate (IRC) calculations were implemented for every located transition state to verify that each TS smoothly connects the corresponding reactant complex and product along the minimum-energy pathway. Electrostatic potential (ESP) was further rendered into colored surface maps via Multiwfn 3.6 and VMD 1.9. The Gibbs free energy variation (ΔG) was employed to evaluate the thermodynamic spontaneity of the ROS-initiated reactions of phenols, while the activation Gibbs free energy barrier ($\Delta G‡$) was defined as the energy difference between a transition state and its preceding reactant complex.

2.6 Cyclic voltammetry

Electrochemical cyclic voltammetry (CV) measurements were carried out on a Zahner PP211 electrochemical workstation equipped with a standard three-electrode configuration: glassy carbon as the working electrode, platinum wire as the counter electrode, and an Ag/Ag^+ electrode as the reference electrode. All CV tests were implemented in 100 μM phenolic sample solutions with 0.1 M $TBAPF_6$ acting as the supporting electrolyte. Voltammograms were acquired at a scan rate of 100 mV s^{-1}. The ferrocene/ferrocenium (Fc/Fc^+) redox pair was adopted as the internal standard for potential calibration. The reported potentials were normalized against the half-wave potential of Fc/Fc^+, whose value is 0.64 V versus the normal hydrogen electrode (NHE).

2.7 Fluorescence Correlation Spectroscopy

Fluorescence correlation spectroscopy (FCS) is a single-molecule analytical technique to examine the microscopic dynamic information of fluorescent dye molecules by recording fluorescence intensity fluctuations within a well-defined confocal detection volume (axial radii, z_0; radial radii, ω_0) [34, 35]. Herein, all FCS experiments were carried out following a slightly modified experimental protocol originally reported by Wiesner et al. [36]. Briefly, the test system contained 10 nM rhodamine 6G (Rh6G) and 10 mM phenolic compounds in a methanol–water mixed solvent (20:80, v/v). All measurements were acquired on a fluorescence lifetime imaging microscope fitted with a 485 nm excitation laser and a Zeiss 100× water-immersion objective (NA = 1.2). Fluorescence emission signals were collected using a 561 nm long-pass optical filter. The autocorrelation curve G(τ) was generated in real time by the hardware correlator from the recorded fluorescence intensity fluctuation traces I(t). Given the intersystem crossing kinetics inherent to Rh6G, the obtained correlation data were fitted to a photophysical model incorporating singlet–triplet conversion processes (Eqs. 3–5).

$$G(\tau) = \frac{[I(t)\cdot I(t+\tau)]}{[I(t)]^2} - 1 \quad \text{(Eq. 3)}$$

$$G(\tau) = \frac{1}{N(1-q)}\left(\frac{1}{1+\frac{\tau}{\tau_D}}\right)\left(\frac{1}{1+\left(\frac{\omega_0}{\omega_z}\right)^2\left(\frac{\tau}{\tau_D}\right)}\right)^{\frac{1}{2}}\left[1-q+q\cdot\exp\left(-\frac{\tau}{\tau_T}\right)\right] \quad \text{(Eq. 4)}$$

$$\tau_{ON} = \frac{\tau_T}{q} \quad \text{(Eq. 5)}$$

Where N denotes the average number of fluorescent molecules within the confocal observation volume; τ_D is the diffusion time, which depends on the structural factor $\omega_0/z_0 = 0.2$; q represents the fraction of fluorophores residing in the triplet state; τ_T refers to the triplet-state decay time; and τ_{ON} denotes the singlet-state residence time.

A reduction in q signifies effective suppression of the triplet-state relaxation pathway, which alleviates oxidative photobleaching accordingly. An elevated τ_{ON} corresponds to an extended fluorescence cycling lifetime ($S_0 \leftrightarrow S_1$). Slight changes in τ_D were tracked to probe possible intermolecular interactions. By systematically correlating these microscale kinetic parameters with macroscopic photostability measurements, the stabilizing effect of different phenolic compounds can be comprehensively elucidated.

3 Results and discussion

3.1 *Para-substituent effects of phenolic compounds on the photostability of Rh6G*

The photostability of Rh6G with various phenolic compounds was assessed by tracking the time-dependent variation in its absorbance at the maximum absorption wavelength. As presented in Fig. S2 and Fig. 2a, the residual rates (RR) of Rh6G upon addition of different phenolic compounds exhibited the following trend: $RR_{Blank} < RR_{PHBA} < RR_{PCP} < RR_{PhOH} < RR_{PEP} < RR_{PAP}$. After 6 h of light irradiation, the RR_{PAP} still remained 79.99%, which was 1.4-fold higher than RR_{Blank} (33.34%). The photodegradation of Rh6G obeyed first-order kinetics. The corresponding calculated degradation rate constants (k) for Blank, PHBA, PCP, PhOH, PEP and PAP were determined to be 0.12379, 0.10371, 0.06888, 0.06248, 0.04907, and 0.03497 h^{-1}, respectively.

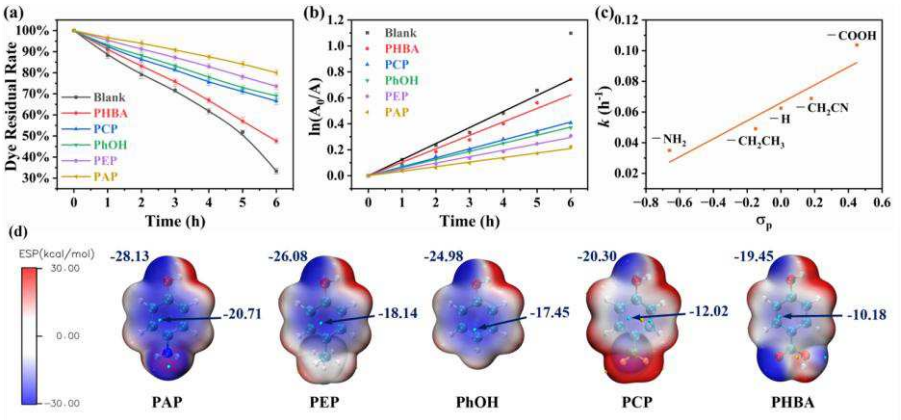

Fig. 2. (a) Time-dependent variation of Rh6G residual rates in the presence of various phenolic compounds under light irradiation. (b) Corresponding degradation rate constants. (c) Correlation between the Hammett substituent constant (σ_p) and k of Rh6G in the presence of different phenolic derivatives. (d) ESP surface distributions of different phenolic compounds. The labelled values represent the local minimum ESP values (unit: kcal/mol) located on the benzene ring of each molecule.

The above results reveal that phenolic compounds exhibit remarkably different efficiencies in improving the photostability of Rh6G. To explore the underlying mechanism, we first investigated the electron-donating and electron-withdrawing properties of various para-substituents. The electronic effect of aromatic substituents can be quantitatively characterized by Hammett substituent constants (σ_p). Specifically, σ_p quantifies the electronic influence of para-substituents: positive values correspond to electron-withdrawing groups (EWGs), while negative values refer to electron-donating groups (EDGs). As reported in previous literature [37], the σ_p values of $-COOH$, $-CH_2CN$, $-H$, $-CH_2CH_3$ and $-NH_2$ were 0.45, 0.18, 0, −0.15 and −0.66, respectively.

To elucidate the influence of these substituents, the correlation curve between σ_p and k was established. Fig. 2c reveals a positive linear correlation between σ_p and k. This trend illustrates the relative difference in protective efficiency among the different phenolic compounds: compared with unsubstituted phenol, para-electron-withdrawing phenolic derivatives offer weaker protection efficacy, resulting in a relatively faster photodegradation of Rh6G. In contrast, para-electron-donating substituents endow phenols with stronger protective performance and achieve a more prominent enhancement in Rh6G photostability. It should be emphasized that all the investigated phenolic compounds can enhance the photostability of Rh6G relative to the blank sample without phenolic additives.

As reported by Ortega-Moo et al. [38], EDGs can raise the electron density of the benzene ring and promote electron donation from the aromatic framework; meanwhile, these substituents also enrich the electron density of phenolic hydroxyl groups, which greatly facilitates thermodynamically favorable proton transfer. In contrast, EWGs reduce the overall molecular electron density of phenolic compounds. These substituent-dependent electronic variations were further verified by electrostatic potential (ESP) surface calculations. As shown in Fig. 2d, the local minimum ESP values of these phenolic molecules gradually become less negative when the para-substituent switches from strong electron-donating $-NH_2$ to strong electron-withdrawing −COOH. It is well recognized that molecules with more negative ESP values exhibit stronger reactivity toward electrophilic reactive oxygen species (ROS) [29, 30]. Nevertheless, the dominant protective mechanism, which may involve electron transfer, proton transfer or direct electrophilic quenching of ROS, still requires systematic investigation.

3.3 Mechanism of photostability improvement induced by phenolic compounds

3.3.1 Capture capacity of ROS

Upon visible light irradiation, dyes produce ROS, such as $^1O_2$, •OH, and$•O_2^-$ [39], which reduce the photostability of dyes by inducing irreversible damage to their molecular structures [40]. Combining with EPR and probe tests (Fig. S3), it was confirmed that photo-generated $^1O_2$ serves as the predominant ROS species accountable for Rh6G degradation, whereas negligible •OH and $•O_2^-$ are produced in this system. To elucidate the mechanism by which phenolic derivatives improve the photostability of Rh6G as well as the differences in their protective efficiency, we conducted EPR measurements and ABDA trapping experiments in the presence of diverse phenolic derivatives.

As shown in Fig. 3a, the blank group (in the absence of phenolic compounds) displayed the highest peak intensity of the TEMP-$^1O_2$ adduct, indicative of the maximum $^1O_2$ generation rate. Upon the

introduction of phenolic compounds, the intensities of these characteristic peaks declined to varying degrees. The $^1O_2$ generation rate was further evaluated via ABDA scavenging experiments. As presented in Fig. S4 and Fig. 3b, the PHBA-containing system showed a slightly lower ABDA residual rate relative to the phenolic-free blank sample, while the PAP group afforded the lowest residual rate. These results demonstrate that phenolic derivatives exert disparate inhibitory effects on $^1O_2$ production. Based on the measured ABDA residual ratios, the $^1O_2$ scavenging capacity of the tested phenolic compounds follows the order: Blank < PHBA < PCP < PhOH < PEP < PAP. This tendency is consistent with the decreasing trend of σ_p values of the para substituents on these phenolic molecules.

$^1O_2$ features vacant antibonding orbitals, which endows it with strong electrophilic reactivity toward electron-rich moieties within molecules. The observed trend in $^1O_2$ quenching is consistent with the gradual decrease in ESP values and further validates the photostability experimental results. Taken together, these results reveal that electron-rich phenolic compounds can effectively scavenge $^1O_2$, thereby significantly enhancing the photostability of Rh6G.

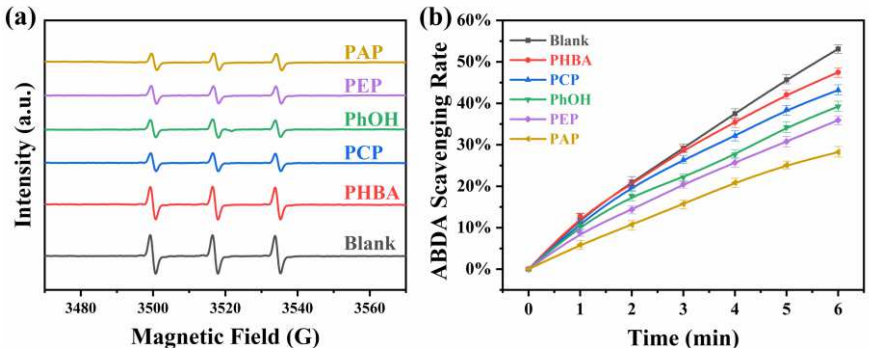

Fig. 3. (a) EPR spectra of Rh6G solution in the present of different phenolic derivatives. (b) ABDA residual rates of Rh6G + ABDA solution under light irradiation in the present of different phenolic derivatives.

3.3.2 DFT calculation of the pathway to quench $^1O_2$

It has been demonstrated that phenolic compounds scavenge $^1O_2$ by forming oxides or peroxides [41–43]. This pathway corresponds to the chemical quenching of $^1O_2$ [44], which can be categorized into four possible reaction modes [45]: (A) formation of allylic hydroperoxides via 1,3-addition; (B) 1,4-cycloaddition to yield 1,4-peroxides; (C) 1,2-cycloaddition accompanied by the generation of 1,2-peroxides; (D) production of hydroperoxy ketones through 1,4-addition. The reaction pathways and corresponding products arising from the interaction between $^1O_2$ and phenolic compounds in this work are illustrated in Fig. 4.

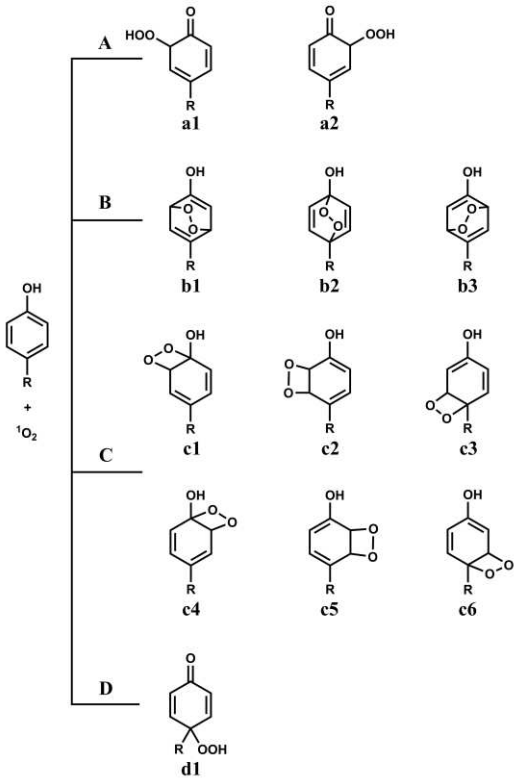

Fig. 4. Four reaction pathways between phenols and $^1O_2$.
(R= -COOH, -CH_2CN, -H, -CH_2CH_3, -NH_2).

First, thermodynamic analysis was performed to assess the spontaneous feasibility of the aforementioned reaction pathways. The Gibbs free energy changes (ΔG) for the reactions of phenolic substrates with $^1O_2$ are listed in Table 1. All routes belonging to Pathway A exhibit negative ΔG values, demonstrating that these processes are thermodynamically spontaneous. By contrast, Pathways B and C yield positive ΔG values, which means the two pathways cannot occur spontaneously under the investigated conditions. As for Pathway D, positive ΔG values are observed for PHBA, PCP and PhOH, while PEP and PAP show negative ΔG. This result indicates that the reactions of PEP and PAP via Pathway D are thermodynamically favorable, whereas the conversion of PHBA, PCP and PhOH are thermodynamically unfavorable.

Table 1. The ΔG values (kcal·mol^{-1}) for all possible reaction pathways between phenols and $^1O_2$.

	PHBA	PCP	PhOH	PEP	PAP
a1	-2.603	-4.171	-5.480	-6.479	-7.070
a2	-3.360	-4.158	-5.471	-6.481	-7.084
b1	23.531	22.573	22.002	19.801	18.208
b2	30.542	16.190	16.178	13.322	12.685

b3	24.587	22.964	23.711	20.868	19.553
c1	19.951	17.872	16.989	15.548	12.496
c2	20.559	20.684	21.016	19.765	19.858
c3	26.782	20.460	21.429	18.274	14.786
c4	17.919	16.126	15.710	14.041	10.713
c5	21.191	21.798	21.470	20.927	20.350
c6	25.986	19.122	19.885	15.989	14.860
d1	12.367	1.467	0.510	-2.485	-1.884

Subsequently, we analyzed the Gibbs free energy barriers of the transition states for each reaction to investigate the differences in reaction rates of various phenolic substrates along the two thermodynamically favorable pathways A and D. In reaction pathway A, $^1O_2$ attacks the carbon atom adjacent to the phenolic hydroxyl group and abstracts a hydrogen atom to ultimately yield an allylic hydroperoxide product. Two distinct products (a1 and a2) are formed owing to the different attack sites of $^1O_2$. The activation Gibbs free energy barriers (ΔG‡) for various para-substituted phenols proceeding via pathway A are summarized in Table 2. Fig. 5c displays the schematic reaction mechanism for this transformation. Employed PHBA as a sample, the optimized geometric structures of the reactant (RC), transition state (TS), and product (P) along the reaction coordinate are presented in Fig. 5d and 5e. The intrinsic reaction coordinate (IRC) calculations further confirm the rationality of these transition-state structures (Fig. S5-9).

For all phenolic substrates, the ΔG‡ values of forming product a1 and a2 are quite close. The slight ΔG‡ discrepancy observed for PHBA can be attributed to the asymmetric spatial configuration of -COOH (Fig. 5d and 5e). As shown in Table 2, the ΔG‡ gradually decreases in the order of PHBA, PCP, PhOH, PEP and PAP, which follows the same trend observed for the Hammett σ_p substituent constant. This finding reveals an intrinsic correlation between the electronic effects of substituents and the kinetic barriers of the investigated reactions. This trend can be rationalized by the more negative electrostatic potential (ESP) distribution on the benzene ring (Fig. 2) originating from electron-donating substituents: the enhanced electrostatic attraction between the electron-rich aromatic ring and electrophilic $^1O_2$ lowers the reaction energy barrier and thus accelerates the reaction rate.

Table 2. ΔG‡ (kcal·mol^{-1}) for TS of reaction A.

	PHBA	PCP	PhOH	PEP	PAP

a1	TS	38.830	37.536	36.225	35.086	31.544
	P	-2.603	-4.171	-5.480	-6.479	-7.070
a2	TS	38.540	37.285	36.232	35.085	31.538
	P	-3.360	-4.158	-5.471	-6.481	-7.084

As illustrated in Fig. 5f-g, Reaction D follows a two-step process. In the first step, $^1O_2$ attacks the benzene ring via transition state TS1 to yield the 4-peroxide intermediate I. The second step proceeds through hydrogen abstraction. Given the large spatial separation between the hydroxyl hydrogen and the peroxide moiety, an additional water molecule is required to mediate hydrogen transfer. Intermediate I thus forms a water-associated complex I-W, which subsequently evolves through transition state TS2 to produce the final ketone hydroperoxide product, accompanied by the release of one water molecule. The energy barrier of TS1 varies between 30.825 to 44.874 kcal·mol^{-1}, whereas the barrier of TS2 ranges from 17.883 to 19.390 kcal·mol^{-1}. Since TS1 possesses a higher energy barrier than TS2, the first step is identified as the rate-determining step for Reaction D. As the Hammett substituent constant σ_p decreases, the energy barrier of TS1 declines (Table 3), leading to an accelerated reaction rate. This phenomenon can be attributed to the more negative ESP distributed over the benzene ring, which facilitates the electrophilic attack of $^1O_2$.

In summary, thermodynamic and kinetic results indicate that all five phenolic substrates (PHBA, PCP, PhOH, PEP and PAP) are reactive along Pathway A, while PEP and PAP can also proceed via Pathway D. Although the availability of this extra reaction pathway for PEP and PAP may further accelerate their reaction rates, it does not alter the relative reactivity order of the five phenolic compounds toward $^1O_2$. Specifically, the reaction rate increases sequentially in the order of PHBA < PCP < PhOH < PEP < PAP.

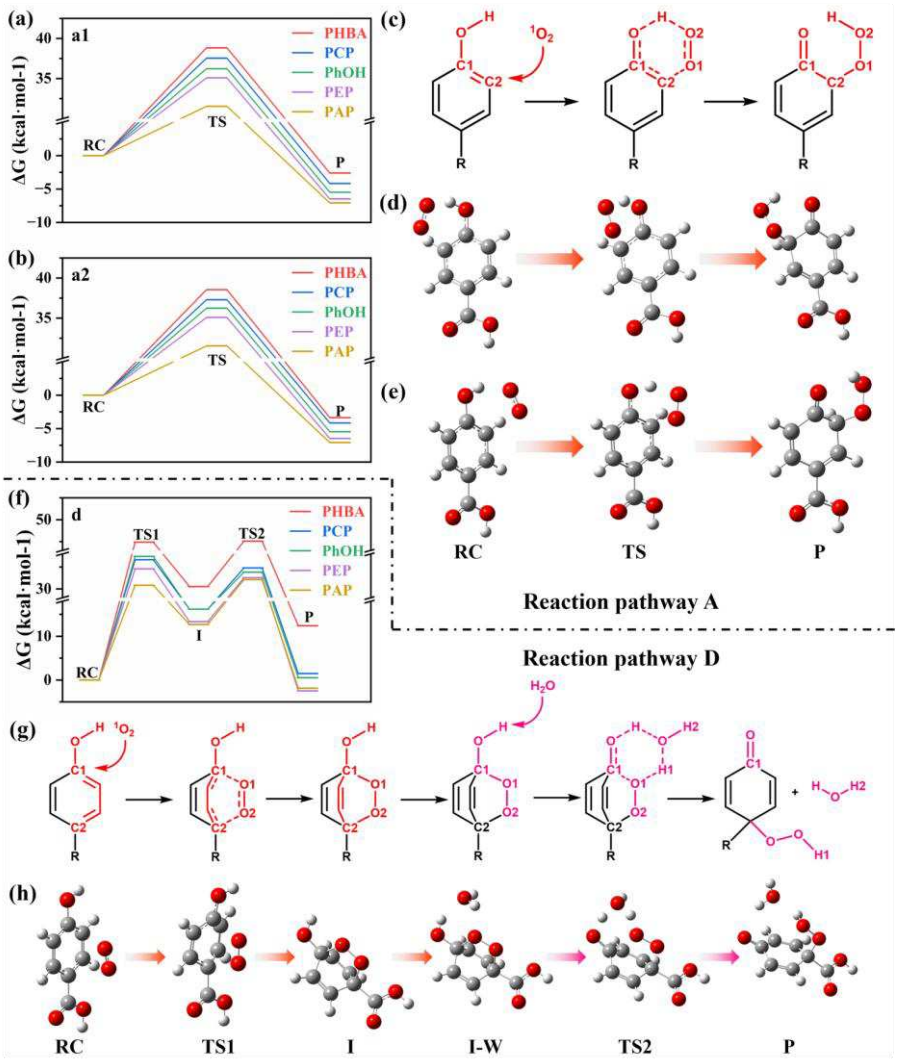

Fig. 5. (a, b) Free energy profiles for $^1O_2$-initiated reaction pathway A of para-substituted phenols: (a) product a1; (b) product a2. (c) Reaction schematic for the $^1O_2$-initiated reaction pathway A. (d, e) Optimized molecular geometries of RC, TS, and P for PHBA para-substitute: Product a1 (d); Product a2 (e). (f) The potential energy surface for reaction D of phenols with $^1O_2$. (g) Reaction schematic for the $^1O_2$-initiated reaction pathway D. (h) The optimized geometries of RC, TS, and P for PHBA para-substitute to product d1.

Table 3. $\Delta G^{\ddagger}$ (kcal·mol^{-1}) of Reaction D between Phenols and $^1O_2$

		PHBA	PCP	PhOH	PEP	PAP
d1	TS1	44.874	36.672	37.408	34.576	30.825
	I	30.542	16.190	16.178	13.322	12.685
	TS2	18.364	18.999	17.883	19.047	19.390
	P	12.367	1.467	0.510	-2.485	-1.884

3.3 3 Antioxidant capacity of various phenolic compounds

Table 4. Antioxidant Capacity and Thermodynamic Parameters of Phenols

Items	PHBA	PCP	PhOH	PEP	PAP
E_{pa}/V	1.758	1.534	1.520	1.415	0.862
HOMO/eV	-0.29207	-0.28248	-0.28154	-0.27205	-0.24422

The mechanism by which phenolic compounds enhance the photostability of Rh6G lies in their effect on scavenging $^1O_2$ generated from the dye under illumination. Specifically, they are preferentially oxidized by $^1O_2$, thus preventing the oxidative degradation of Rh6G. Their protective ability is positively correlated with reducing capacity: phenols with stronger reducing power more effectively inhibit Rh6G photobleaching. Herein, we evaluated the reducing capacity of these phenolic compounds via cyclic voltammetry (CV) measurements and theoretical HOMO energy level calculations.

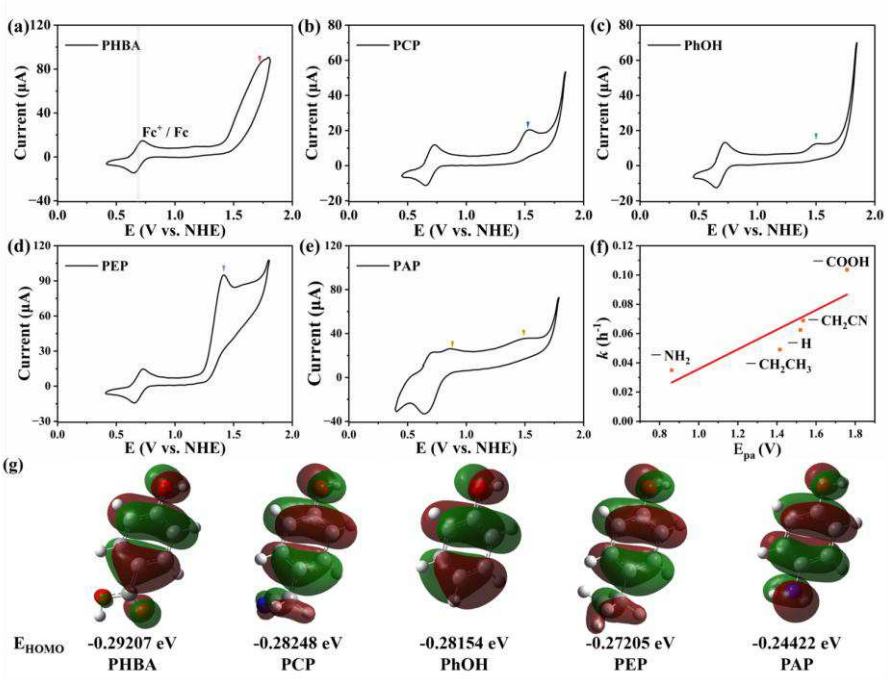

Fig. 6. (a–e) Cyclic voltammograms of various phenolic compounds measured in methanol solution (the central redox peak corresponds to the fc/fc$^+$ couple). (f) Correlation between the degradation rate constant *k* of Rh6G and E_{pa} of phenolic compounds. (g) HOMO electron density isosurfaces and energy levels of various phenolic compounds.

Fig. 6a–e show the cyclic voltammograms of different phenolic compounds recorded in methanol. As summarized in Table 4, the first anodic peak potentials (E_{pa}) of PHBA, PCP, PhOH, PEP and PAP are 1.758, 1.534, 1.520, 1.415 and 0.862 V, respectively. The E_{pa} values show a positive correlation with the degradation rate of Rh6G in the presence of each phenolic additive (Fig. 6f). As presented in Fig. 6g and Table 4, the HOMO energy levels of these phenolic compounds increase in the following order: PHBA

(−0.29207 eV) < PCP (−0.28248 eV) < PhOH (−0.28154 eV) < PEP (−0.27205 eV) < PAP (−0.24422 eV). These results demonstrate that the reducing capacity of these phenolic compounds follows the sequence: PHBA < PCP < PhOH < PEP < PAP, which is in good agreement with the electron-donating ability of the phenolic molecules.

3.3.5 Fluorescence correlation spectroscopy test

To more deeply elucidate the mechanism and efficiency by which phenolic compounds enhance the photostability of Rh6G, we investigated the real-time photobleaching kinetics of Rh6G via fluorescence correlation spectroscopy (FCS). The fitted G(τ) autocorrelation curves of Rh6G upon the addition of various phenolic compounds are shown in Fig. S10 and summarized in Fig. 7a. In the time range of 10^{-4}-10^{-3} ms, the blank Rh6G solution exhibited the largest amplitude, indicative of its highest triplet-state proportion. The addition of phenolic compounds led to an obvious reduction in curve amplitude, demonstrating that these phenols can effectively suppress the triplet-state population of Rh6G.

As listed in Table 5, the triplet-state ratio q of Rh6G follows the sequence: q_{Blank} (79.45%) > q_{PHBA} (74.93%) > q_{PCP} (71.49%) > q_{PhOH} (63.12%) > q_{PEP} (56.98%) > q_{PAP} (49.37%). Meanwhile, the τ_{ON} values of Rh6G molecules in different solutions rank in the order: $\tau_{ON\text{-}Blank}$ (0.21963 μs) < $\tau_{ON\text{-}PHBA}$ (0.27854 μs) < $\tau_{ON\text{-}PCP}$ (0.33793 μs) < $\tau_{ON\text{-}PhOH}$ (0.55397 μs) < $\tau_{ON\text{-}PEP}$ (0.71696 μs) < $\tau_{ON\text{-}PAP}$ (1.07961 μs). Collectively, the trends of q and τ_{ON} results reveal that the triplet-state ratio of Rh6G in the presence of different phenolic compounds decreases in the order: Blank > PHBA > PCP > PhOH > PEP > PAP. Given that the T_1-state Rh6G reacts with ground-state oxygen to generate $^1O_2$, the yield of $^1O_2$ is positively correlated with T_1-state population. Accordingly, the regulatory effect of various phenolic compounds on $^1O_2$ yield is consistent with their influence on the triplet-state ratio of Rh6G.

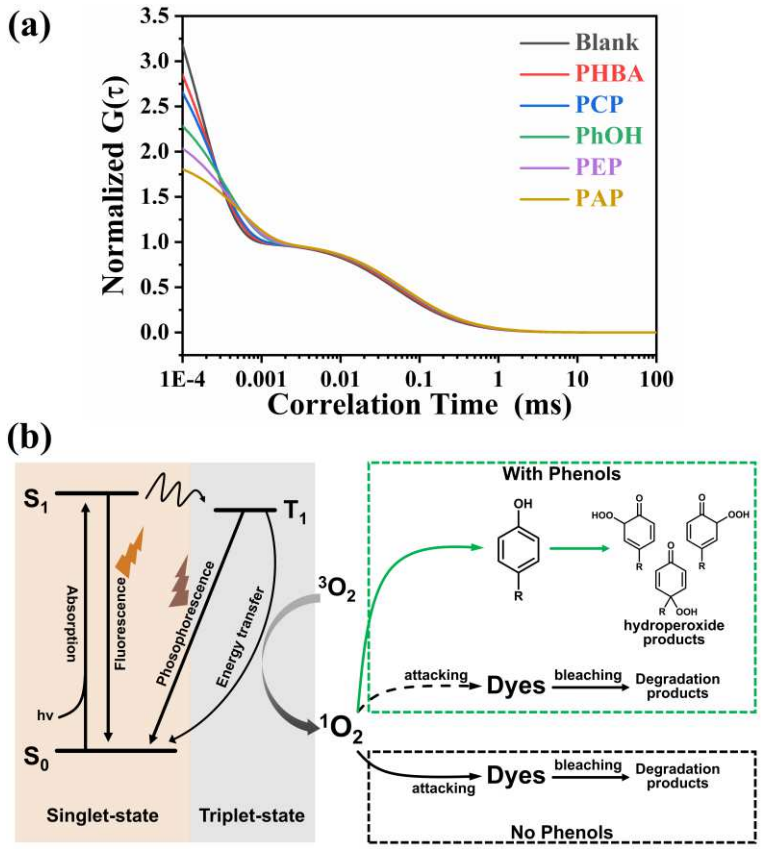

Fig. 7. (a) G(τ) curves of Rh6G dye solution and with phenols.
(b) Mechanism of phenolic compounds in enhancing the photostability of Rh6G dye.

Table 5. The fitting parameters of G(τ)

	Blank	PHBA	PCP	PhOH	PEP	PAP
q	79.45%	74.93%	71.49%	63.12%	56.98%	49.37%
τ_{ON} (μs)	0.21963	0.27854	0.33793	0.55397	0.71696	1.07961

Based on the above investigations, we herein propose a mechanism by which phenolic compounds enhance the photostability of Rh6G, and elaborate on how the electronic properties of para-substituents on phenolic hydroxyl groups govern their protective efficiency. As depicted in Fig. 7b, upon light irradiation, Rh6G molecules are excited from the ground state (S_0) to the first singlet excited state (S_1) or higher-lying singlet excited states (S_2, S_3, etc.). Molecules populated in high-energy excited states rapidly relax to the S_1 state via non-radiative transitions. A fraction of these S_1-state molecules returns to the S_0 state through fluorescence emission, while the remaining S_1-state species undergo intersystem crossing to populate the T_1 state. T_1-state molecules can decay back to the ground state by releasing

phosphorescence or thermal energy; alternatively, they react with triplet oxygen ($^3O_2$) to generate $^1O_2$, which is responsible for the photobleaching of Rh6G.

In the presence of phenolic compounds, these species competitively scavenge $^1O_2$ against Rh6G. Phenolic derivatives protect the Rh6G dye via a sacrificial antioxidant mechanism: the phenols are preferentially oxidized to consume reactive $^1O_2$, thereby mitigating Rh6G photodegradation. A higher reaction reactivity of phenols toward $^1O_2$ corresponds to a more pronounced improvement in the photostability of Rh6G.

With regard to the substituent effect at the para position of the phenolic hydroxyl group: stronger electron-donating para-substituents reduce the activation energy for the addition reaction between phenols and $^1O_2$, accelerating the reaction rate and thus affording superior protective performance for the dye. In contrast, para-substituents with strong electron-withdrawing character elevate the activation energy of the phenol–$^1O_2$ addition reaction, slowing down the reaction kinetics and consequently weakening their capability to enhance dye photostability.

4 Conclusion

In summary, five phenolic derivatives with different para-substitutes (PHBA, PCP, PhOH, PEP and PAP) were employed to explore how substituent electronic properties modulate the photostability of Rh6G upon 532 nm laser irradiation. All these phenolic derivatives improve the photostability of Rh6G, and their protective efficiency follows the trend: PHBA < PCP < PhOH < PEP < PAP. Their protective efficacy exhibits a linear correlation with their σ_p: relative to unsubstituted phenol, para-electron-withdrawing substituents weaken the protective performance, whereas para-electron-donating substituents afford stronger protection.

EPR and radical trapping experiments confirm that $^1O_2$ is the dominant reactive oxygen species responsible for Rh6G photobleaching and these phenolic additives can effectively quench $^1O_2$. Mechanistic investigations show that the phenols protect Rh6G dye by acting as sacrificial agents that react with $^1O_2$. The CV measurements and HOMO energy level calculations disclosed that the protection efficacy of these phenols is positively correlated with their reducing capacity, following the same order: PHBA < PCP < PhOH < PEP < PAP. DFT calculations indicate that the chemical quenching of $^1O_2$ proceeds mainly via 1,3-addition to generate allylic hydroperoxides; an alternative 1,4-addition pathway

is accessible only for PEP and PAP. The reaction barrier declines ad σ_p decrease, which arises from strengthened electrostatic attraction between the electron-rich aromatic ring and electrophilic $^1O_2$. Fluorescence correlation spectroscopy further demonstrated that the phenols decrease the triplet-state population and the regulatory effect of these phenols on $^1O_2$ yield matches their impact on the triplet-state fraction of Rh6G.

These findings demonstrate that incorporating phenolic additives bearing stronger para-electron-donating substituents constitutes an effective strategy to enhance the photostability of Rh6G. This work is anticipated to be extendable to other dye platforms and provides guidance for the rational design of dye photostabilizers.

Supplementary Information

The online version contains supplementary material available at https://doi.org/

Acknowledgements

This research was funded by the Fundamental Research Funds for the Central Universities (JKD01261701, 222201717003) and the Science and Technology Commission of Shanghai Municipality (22230780200, 20DZ2250400).

Author contributions

Runxin Wang: Writing–original draft, Methodology, Formal analysis, Data curation. Liang Sun: Data curation. Yudong Liu: Investigation, Data curation. Jinlong Zhang: Supervision. Baozhu Tian: Writing–review & editing, Supervision, Conceptualization.

Data availability

No datasets were generated or analysed during the current study.

Declarations

Conflict of interest

The authors declare no competing interests.

References

[1] Wu, L., Wang, X., Huang, J., Wei, H., & Kan, C. (2022). Switch-type near-infrared fluorescent probes for Hg^{2+} based on rhodamines. *Journal of Photochemistry and Photobiology A: Chemistry, 429*, 113936. https://doi.org/10.1016/j.jphotochem.2022.113936

[2] Xiang, F.-F., Zhang, H., Wu, Y.-L., Chen, Y.-J., Liu, Y.-Z., Chen, S.-Y., Guo, Y.-Z., Yu, X.-Q., & Li, K. (2024). Machine-learning-assisted rational design of Si-rhodamine as cathepsin-pH-activated probe for accurate fluorescence navigation. *Advanced Materials, 36*(31), 2404828. https://doi.org/10.1002/adma.202404828

[3] Beija, M., Afonso, C. A. M., & Martinho, J. M. G. (2009). Synthesis and applications of rhodamine derivatives as fluorescent probes. *Chemical Society Reviews, 38*(8), 2410–2433. https://doi.org/10.1039/b901612k

[4] Han, W., Zhang, X., Chen, M., Chu, X., Li, W., Fu, P., Jia, Z., & Li, Y. (2023). Construction of multilayered boron nitride nanosheets for improving optical performance and stability of rhodamine B. *Dyes and Pigments, 215*, 111244. https://doi.org/10.1016/j.dyepig.2023.111244

[5] Lee, Y., Yu, S. H., Jeon, J., Kim, H., Lee, J. Y., Kim, H., Ahn, J.-H., Hwang, E., & Cho, J. H. (2015). Hybrid structures of organic dye and graphene for ultrahigh gain photodetectors. *Carbon, 88*, 165–172. https://doi.org/10.1016/j.carbon.2015.02.071

[6] Ratanpara, A., Kim, M., Kim, Y. J., & Hidrovo, C. H. (2025). Spectral characteristics of water-soluble rhodamine derivatives for laser-induced fluorescence. *Journal of Fluorescence, 35*(6), 4143–4155. https://doi.org/10.1007/s10895-024-03819-1

[7] Fang, Y., Cheng, J., Wang, S., & Xu, L. (2025). Tunable dye laser for application in laser display technology. *Optics & Laser Technology, 192*, 114113. https://doi.org/10.1016/j.optlastec.2025.114113

[8] Zhang, Y., Ren, X., Zhao, X., Ding, S., Wu, X., Liu, Y., Zeng, X., Qu, X., Song, H., Hu, Y., Shi, L., & Lu, S. (2025). Rhodamine B-derived low-toxicity full-color carbon dots with wide tunable high-stable liquid-state lasers. *Advanced Materials, 37*(13), 2420197. https://doi.org/10.1002/adma.202420197

[9] Li, Y., Li, S., Huang, Z., Zhang, D., & Jia, Q. (2024). Research progress of fluorescent composites based on cyclodextrins: Preparation strategies, fluorescence properties and applications in sensing and bioimaging. *Analytica Chimica Acta, 1316*, 342878. https://doi.org/10.1016/j.aca.2024.342878

[10] Li, S., Huo, F., & Yin, C. (2022). Progress in the past five years of small organic molecule dyes for tumor microenvironment imaging. *Chemical Communications, 58*(91), 12642–12652. https://doi.org/10.1039/d2cc04975a

[11] Kim, H. N., Lee, M. H., Kim, H. J., Kim, J. S., & Yoon, J. (2008). A new trend in rhodamine-based chemosensors: Application of spirolactam ring-opening to sensing ions. *Chemical Society Reviews, 37*(8), 1465–1472. https://doi.org/10.1039/b802497a

[12] Song, L., Hennink, E. J., Young, I. T., & Tanke, H. J. (1995). Photobleaching kinetics of fluorescein in quantitative fluorescence microscopy. *Biophysical Journal, 68*(6), 2588–2600. https://doi.org/10.1016/s0006-3495(95)80442-x

[13] Zhang, J., Zhang, K., Wang, K., Wang, B., Zhu, S., Qian, H., Ma, Y., Zhang, M., Liu, T., Chen, P., Shen, Y., Fu, Y., Fang, S., Zhang, X., Zou, P., Deng, W., Mu, Y., & Chen, Z. (2025). A palette of bridged bicycle-strengthened fluorophores. *Nature Methods, 22*(6), 1276–1287. https://doi.org/10.1038/s41592-025-02693-4

[14] Yao, Y., Xiao, X., Liu, S., Tian, B., & Zhang, J. (2023). Syntheses, optical properties, and bioimaging application of near-infrared aza-BODIPY dyes with electronic push–pull system. *Research on Chemical Intermediates, 49*(7), 2955–2968. https://doi.org/10.1007/s11164-023-05028-0

[15] Liu, Y., Chen, F., Sun, L., Zhang, Z., Chang, S., Zhang, J., & Tian, B. (2023). Influences of molecular structures on the spectral properties and photostability of rhodamine dyes. *Research on Chemical Intermediates, 49*(6), 2417–2432. https://doi.org/10.1007/s11164-023-05016-4

[16] Liu, Y., Liu, S., Miao, R., Sun, L., Zhang, Z., Chen, F., Zhang, J., Li, S., & Tian, B. (2023). Insight into the relationship between the photostability and molecular structure of rhodamine dyes. *Tetrahedron, 149*, 133664. https://doi.org/10.1016/j.tet.2023.133664

[17] Ran, X., Lin, W., Song, K., Cao, S., Sun, L., Liu, Y., Tian, B., & Zhang, J. (2026). Esterification engineering of rhodamine dyes: Enhancing spectral tunability, solvent applicability, and chemo/photostability. *Research on Chemical Intermediates, 52*(6), 4105–4125. https://doi.org/10.1007/s11164-025-05869-x

[18] Su, L., Shu, L., Shi, B., Hang, Y., & Huang, J. (2021). Construction of enhanced photostability anthraquinone-type nanovesicles based on a novel two-step supramolecular assembly strategy and their application on multiband laser-responsive composites. *ACS Applied Materials & Interfaces, 13*(36), 43458–43472. https://doi.org/10.1021/acsami.1c14352

[19] Yue, Y., Xu, Z., Ma, K., Huo, F., Qin, X., Zhang, K., & Yin, C. (2024). HSA shrinkage optimizes the photostability of embedded dyes fundamentally to amplify their efficiency as photothermal materials. *Chinese Chemical Letters, 35*(8), 109223. https://doi.org/10.1016/j.cclet.2023.109223

[20] Barulin, A., & Wenger, J. (2020). Ultraviolet photostability improvement for autofluorescence correlation spectroscopy on label-free proteins. *The Journal of Physical Chemistry Letters, 11*(6), 2027–2035. https://doi.org/10.1021/acs.jpclett.0c00209

[21] Giloh, H., & Sedat, J. W. (1982). Fluorescence microscopy: Reduced photobleaching of rhodamine and fluorescein protein conjugates by n-propyl gallate. *Science, 217*(4566), 1252–1255. https://doi.org/10.1126/science.7112126

[22] Haimerl, J. M., Ghosh, I., König, B., Lupton, J. M., & Vogelsang, J. (2018). Chemical photocatalysis with rhodamine 6G: Investigation of photoreduction by simultaneous fluorescence correlation spectroscopy and fluorescence lifetime measurements. *The Journal of Physical Chemistry B, 122*(47), 10728–10735. https://doi.org/10.1021/acs.jpcb.8b08615

[23] Aitken, C. E., Marshall, R. A., & Puglisi, J. D. (2008). An oxygen scavenging system for improvement of dye stability in single-molecule fluorescence experiments. *Biophysical Journal, 94*(5), 1826–1835. https://doi.org/10.1529/biophysj.107.117689

[24] Liu, Y., Ning, L., Luo, Y., Huang, Y., He, Z., Ma, H., Zhao, Y., Zhang, J., Liu, D., Fu, L., Langford, S. J., Gale, P. A., Luo, Y., & Bao, G. (2024). Stabilizing dye-sensitized upconversion hybrids by cyclooctatetraene. *Nano Letters, 24*(40), 12486–12492. https://doi.org/10.1021/acs.nanolett.4c03391

[25] Wang, P. Y., Chen, Y. P., & Yang, P. Z. (1996). The effect of a UV-absorber on the photostability of acid dyes on silk. *Dyes and Pigments, 30*(2), 141–149. https://doi.org/10.1016/0143-7208(95)00077-1

[26] Kohno, Y., Kato, Y., Shibata, M., Fukuhara, C., Maeda, Y., Tomita, Y., & Kobayashi, K. (2015). Enhanced stability of natural anthocyanin incorporated in Fe-containing mesoporous silica. *Microporous and Mesoporous Materials, 203*, 232–237. https://doi.org/10.1016/j.micromeso.2014.10.042

[27] Gamage, R. S., & Smith, B. D. (2022). Spontaneous transfer of indocyanine green from liposomes to albumin is inhibited by the antioxidant α-tocopherol. *Langmuir, 38*(39), 11950–11961. https://doi.org/10.1021/acs.langmuir.2c01715

[28] Zha, X., Wang, R., Chen, Q., Liu, Y., Sun, L., Zhang, J., & Tian, B. (2026). Investigating the mechanism and potency of phenolic additives in enhancing the photostability of rhodamine 6G: Scavenging its triplet state and inhibiting singlet oxygen formation. *Journal of Photochemistry and Photobiology A: Chemistry, 473*, 116869. https://doi.org/10.1016/j.jphotochem.2025.116869

[29] Elovitz, M. S., & Fish, W. (1995). Redox interactions of Cr(VI) and substituted phenols: Products and mechanism. *Environmental Science & Technology, 29*(8), 1933–1943. https://doi.org/10.1021/es00008a010

[30] Elovitz, M. S., & Fish, W. (1994). Redox interactions of Cr(VI) and substituted phenols: Kinetic investigation. *Environmental Science & Technology, 28*(12), 2161–2169. https://doi.org/10.1021/es00061a026

[31] Yang, J., Chen, J., Hao, Y., & Liu, Y. (2021). Identification of the DPPH radical scavenging reaction adducts of ferulic acid and sinapic acid and their structure-antioxidant activity relationship. *LWT, 146*, 111411. https://doi.org/10.1016/j.lwt.2021.111411

[32] Shang, Y., Li, X., Li, Z., Shen, L., Zhou, J., Hu, R., & Chen, K. (2022). Mechanistic study on the radical scavenging activity of viniferins. *Journal of Molecular Structure, 1260*, 132830. https://doi.org/10.1016/j.molstruc.2022.132830

[33] Yang, J., Lv, G., & Sun, X. (2024). Singlet oxygen and hydroxyl radical in the transformation of acetaminophen in surface water: The mechanism on the degradation pathways based on DFT calculations. *Journal of Environmental Chemical Engineering, 12*(6), 114933. https://doi.org/10.1016/j.jece.2024.114933

[34] Widengren, J., Dapprich, J., & Rigler, R. (1997). Fast interactions between Rh6G and dGTP in water studied by fluorescence correlation spectroscopy. *Chemical Physics, 216*(3), 417–426. https://doi.org/10.1016/s0301-0104(97)00014-1

[35] Widengren, J., Chmyrov, A., Eggeling, C., Löfdahl, P.-Å., & Seidel, C. A. M. (2007). Strategies to improve photostabilities in ultrasensitive fluorescence spectroscopy. *The Journal of Physical Chemistry A, 111*(3), 429–440. https://doi.org/10.1021/jp0646325

[36] Kohle, F. F. E., Hinckley, J. A., & Wiesner, U. B. (2019). Dye encapsulation in fluorescent core–shell silica nanoparticles as probed by fluorescence correlation spectroscopy. *The Journal of Physical Chemistry C, 123*(15), 9813–9823. https://doi.org/10.1021/acs.jpcc.9b00297

[37] Monteiro-de-Castro, G., Duarte, J. C., & Borges, I., Jr. (2023). Machine learning determination of new Hammett's constants for meta- and para-substituted benzoic acid derivatives employing quantum chemical atomic charge methods. *The Journal of Organic Chemistry, 88*(14), 9791–9802. https://doi.org/10.1021/acs.joc.3c00410

[38] Ortega-Moo, C., Garza, J., & Vargas, R. (2016). The substituent effect on the antioxidant capacity of catechols and resorcinols. *Theoretical Chemistry Accounts, 135*(7), 177. https://doi.org/10.1007/s00214-016-1932-7

[39] Konstantinou, I. K., & Albanis, T. A. (2004). TiO_2-assisted photocatalytic degradation of azo dyes in aqueous solution: Kinetic and mechanistic investigations: A review. *Applied Catalysis B: Environmental, 49*(1), 1–14. https://doi.org/10.1016/j.apcatb.2003.11.010

[40] DeRosa, M. C., & Crutchley, R. J. (2002). Photosensitized singlet oxygen and its applications. *Coordination Chemistry Reviews, 233–234*, 351–371. https://doi.org/10.1016/s0010-8545(02)00034-6

[41] Tsuchida, K., Okumura, H., Ikarashi, T., & Takahashi, Y. (2022). Chlorogenic acids protect organic dyes against self-catalyzed photobleaching. *Journal of Photochemistry and Photobiology A: Chemistry, 433*, 114163. https://doi.org/10.1016/j.jphotochem.2022.114163

[42] Al-Nu'airat, J., Dlugogorski, B. Z., Gao, X., Zeinali, N., Skut, J., Westmoreland, P. R., Oluwoye, I., & Altarawneh, M. (2019). Reaction of phenol with singlet oxygen. *Physical Chemistry Chemical Physics, 21*(1), 171–183. https://doi.org/10.1039/c8cp04852e

[43] Kim, J. I., Lee, J. H., Choi, D. S., Won, B. M., Jung, M. Y., & Park, J. (2009). Kinetic study of the quenching reaction of singlet oxygen by common synthetic antioxidants (tert-butylhydroxyanisol, tert-di-butylhydroxytoluene, and tert-butylhydroquinone) as compared with α-tocopherol. *Journal of Food Science, 74*(5), C362–C369. https://doi.org/10.1111/j.1750-3841.2009.01160.x

[44] Rawls, H. R., & Van Santen, P. J. (1970). A possible role for singlet oxygen in the initiation of fatty acid autoxidation. *Journal of the American Oil Chemists' Society, 47*(4), 121–125. https://doi.org/10.1007/bf02640400

[45] Bobrowski, M., Liwo, A., Ołdziej, S., Jeziorek, D., & Ossowski, T. (2000). CAS MCSCF/CAS MCQDPT2 study of the mechanism of singlet oxygen addition to 1,3-butadiene and benzene. *Journal of the American Chemical Society, 122*(34), 8112–8119. https://doi.org/10.1021/ja001185c

Graphic abstract

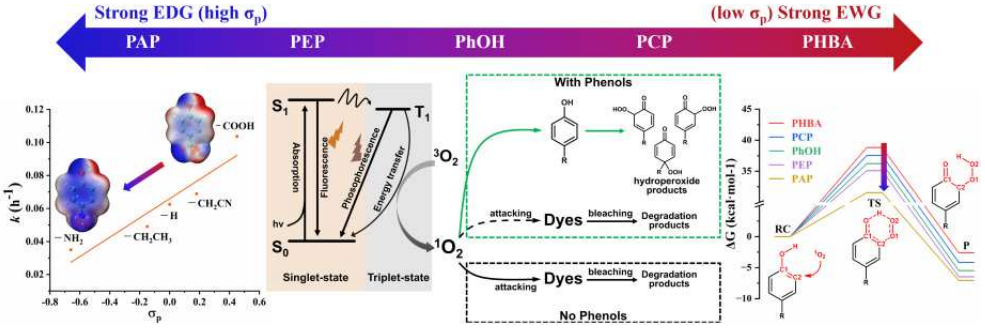

Modulating the electron-donating ability of phenolic *para*-substituents is the decisive fundamental mechanism for enhancing their efficacy of Rh6G photostability. By lowering the Gibb free energy barrier for phenols reacting with $^1O_2$, phenols with strong EDG (high σ_p) effectively quench $^1O_2$, thereby blocking the photobleaching of dyes.

Supplementary Files

This is a list of supplementary files associated with this preprint. Click to download.

- SI.docx